Molecular Magnetic Resonance Imaging of Pulmonary Fibrosis in Mice

Peter Caravan[1], Yan Yang[1], Roshini Zachariah[2], Anthony Schmitt[2], Mari Mino-Kenudson[3], Howard H. Chen[1], David E. Sosnovik[1], Guangping Dai[1], Bryan C. Fuchs[4], and Michael Lanuti[2]

[1]A. A. Martinos Center for Biomedical Imaging, Department of Radiology, Massachusetts General Hospital and Harvard Medical School, Charlestown, Massachusetts; [2]Division of Thoracic Surgery, Massachusetts General Hospital and Harvard Medical School, Boston, Massachusetts; [3]Division of Pathology, Massachusetts General Hospital, Boston, Massachusetts; and [4]Division of Surgical Oncology, Massachusetts General Hospital Cancer Center and Harvard Medical School, Boston, Massachusetts

Idiopathic pulmonary fibrosis is a chronic, progressive, fibrosing interstitial pneumonia of unknown cause resulting in dyspnea and functional decline until death. There are currently no effective noninvasive tools to monitor disease progression and response to treatment. The objective of the present study was to determine whether molecular magnetic resonance imaging of the lung using a probe targeted to type I collagen could provide a direct, noninvasive method for assessment of pulmonary fibrosis in a mouse model. Pulmonary fibrosis was generated in mice by transtracheal instillation of bleomycin (BM). Six cohorts were imaged before and immediately after intravenous administration of molecular imaging probe: (*1*) BM plus collagen-targeted probe, EP-3533; (*2*) sham plus EP-3533; (*3*) BM plus nonbinding control probe, EP-3612; (*4*) sham plus EP-3612; (*5*) BM plus EP-3533 imaged early; and (*6*) BM plus EP-3533 imaged late. Signal-to-noise ratio (SNR) enhancement was quantified in the lungs and muscle. Lung tissue was subjected to pathologic scoring of fibrosis and analyzed for gadolinium and hydroxyproline. BM-treated mice had 35% higher lung collagen than sham mice ($P < 0.0001$). The SNR increase in the lungs of fibrotic mice after EP-3533 administration was twofold higher than in sham animals and twofold higher than in fibrotic or sham mice that received control probe, EP-3612 ($P < 0.0001$). The SNR increase in muscle was similar for all cohorts. For EP-3533, we observed a strong, positive, linear correlation between lung SNR increase and hydroxyproline levels ($r = 0.72$). Collagen-targeted probe EP-3533–enhanced magnetic resonance imaging specifically detects pulmonary fibrosis in a mouse model of disease.

Keywords: molecular imaging; gadolinium; type I collagen; bleomycin; EP-3533

CLINICAL RELEVANCE

There are currently no effective noninvasive tools to monitor pulmonary fibrosis progression or response to treatment. This study demonstrates the specificity of a collagen-targeted magnetic resonance imaging probe to noninvasively identify pulmonary fibrosis in a mouse model of the disease.

Idiopathic pulmonary fibrosis (IPF) is a chronic, progressive, fibrosing interstitial pneumonia of unknown cause that primarily affects older adults. In the majority of cases, it is a relentlessly progressive disease that results in dyspnea and functional decline until death. The median survival remains unacceptably poor, at approximately 2–3 years (1, 2). A recent analysis based on healthcare claims data of a large health plan in the United States yielded a prevalence estimate of between 14.0 and 42.7 per 100,000 persons, depending on the case definition used (3), which translates to a range of 44,000–134,000 affected Americans based on the current population. Currently, there is no effective treatment for the disease (4). Lung transplantation has been employed in carefully selected patients. Progress has been hampered by the lack of noninvasive methods for diagnosis and the lack of methods for monitoring the progression of the disease. Although high-resolution computed tomography (HRCT) scanning has proven invaluable in the diagnosis of the disease (5), up to 50% of patients do not have clear radiologic hallmarks of fibrosis, such as honeycombing, subpleural lower lobe reticular opacities, or traction bronchiectasis, and these cases require lung biopsy for diagnosis (6). Even when a surgical lung biopsy is possible, there is also the possibility of sampling error despite sampling multiple lobes (7, 8). Once the diagnosis has been made with reasonable certainty, tracking disease progression can be problematic, and physiological changes are often only noted with acute exacerbations. This difficulty in disease monitoring is highlighted by the numerous endpoints that have been chosen in clinical trials, such as forced vital capacity, diffusing capacity, arterial oxygen pressure, 6-minute walk test, survival, and progression-free survival (9). It is clear that new methods of diagnosis and monitoring in IPF are needed.

Overexpression of collagen is a hallmark of fibrosis. Here, we hypothesized that molecular magnetic resonance imaging (MRI) with a probe targeted to type I collagen could provide a noninvasive method for assessment of fibrosis. EP-3533 is a gadolinium (Gd)-based probe designed to specifically target type I collagen that has previously demonstrated its utility in MRI of cardiac and hepatic fibrosis (10–13). MR proton imaging of the lung is less common, due to the lower proton density and because of the short T2 relaxation times in the lung, both of which result in MR signal loss. However, new MRI pulse sequences, such as the ultrashort echo time (UTE) sequence, now make lung imaging more feasible (14). The goal of this study was to assess the feasibility of EP-3533–enhanced MRI to quantify collagen in the lung, and to determine whether collagen-targeted MRI has the potential to act as a noninvasive measure of pulmonary fibrosis.

(*Received in original form January 25, 2013 and in final form July 22, 2013*)

This work was supported by National Heart, Lung, and Blood Institute and the National Institute of Biomedical Imaging and Bioengineering grants HL116315 and EB009062 (P.C.).

Author Contributions: Conception and design of study (P.C., D.E.S., B.C.F., M.L.); acquisition of data (P.C., Y.Y., R.Z., A.S., G.D., H.H.C.); analysis and interpretation of data (all authors); P.C. drafted the article and all authors contributed to the critical revision for content; all authors gave final approval of the version to be published.

Correspondence and requests for reprints should be addressed to Peter Caravan, Ph.D., A. A. Martinos Center for Biomedical Imaging, Department of Radiology, Massachusetts General Hospital and Harvard Medical School, 149 13th Street, Suite 2301, Charlestown, MA 02129. E-mail: caravan@nmr.mgh.harvard.edu

This article has an online supplement, which is accessible from this issue's table of contents at www.atsjournals.org

Am J Respir Cell Mol Biol Vol 49, Iss. 6, pp 1120–1126, Dec 2013

Originally Published in Press as DOI: 10.1165/rcmb.2013-0039OC on August 8, 2013
Internet address: www.atsjournals.org

MATERIALS AND METHODS

Animal Model

All experiments were performed in accordance with National Institutes of Health guidelines for the care and use of laboratory animals, and were approved by the institution's animal care and use committee. Pulmonary fibrosis was initiated in 10-week-old male C57/BL6 mice by transtracheal administration of bleomycin (BM; 2.5 U/kg) in PBS. Sham animals received only PBS.

Probes

EP-3533 comprises a 10–amino acid cyclic peptide conjugated to three Gd moieties with affinity for type I collagen ($K_d = 1.8$ μM) and strong MR signal enhancement (relaxivity = 16.2 mM^{-1} s^{-1} [5.4/Gd ion] at 4.7T) (12). EP-3612 has an identical structure to EP-3533, except that one of the cysteine moieties is changed from L-Cys in EP-3533 to D-Cys in EP-3612. This change in chirality results in a greater than 100-fold loss in collagen affinity for EP-3612; however, its relaxivity remains equivalent to EP-3533. Probes were synthesized as described previously (11).

MRI and Analysis

Mice were divided into four cohorts: (*1*) BM plus collagen-targeted probe, EP-3533 ($n = 6$); (*2*) sham plus EP-3533 ($n = 5$); (*3*) BM plus nonbinding control probe, EP-3612 ($n = 5$); and (*4*) sham plus EP-3612 ($n = 5$). Mice were imaged 9–11 days after BM instillation. We imaged an additional two groups of animals with EP-3533 at 5–6 days ($n = 4$) or 12–14 days ($n = 5$) after BM instillation.

The imaging protocol involved: (*1*) multislice two-dimensional rapid acquisition with refocused echo (RARE) imaging to delineate anatomy; (*2*) a baseline three-dimensional (3D) UTE sequence with respiratory gating (repeated at 12 min after injection); (*3*) a baseline 3D fast low-angle shot (FLASH) angiography sequence (repeated five times); and (*4*) bolus injection of 10 μmol/kg of either EP-3533 or EP-3612.

Images were analyzed using the program Osirix (www.osirix-viewer.com/). For the pre- and post-probe UTE images, regions of interest (ROIs) were drawn in the lung, the shoulder muscle, and in the air adjacent to the animal. For each slice, the signal intensity (SI) in the lung and muscle was obtained. The standard deviation (SD) of the SI in the air adjacent to the animal was used to estimate the noise. For each image slice, pre- and post-probe, signal-to-noise ratio (SNR) was calculated as $SNR = SI_{tissue}/SD_{air}$.

The percent increase in signal post probe was calculated as:

$$\%\text{Signal increase} = (SNR_{Post} - SNR_{Pre})/SNR_{Pre} \times 100\%$$

Tissue Analysis

The right lung was inflated and fixed with 10% formalin, embedded in paraffin, cut into 5-μm-thick sections, and stained with hematoxylin and eosin, trichrome, and Sirius red, with a counterstain of Fast Green. Sirius red–stained sections were analyzed using ImageJ (rsbweb.nih.gov/ij/). The left lung was digested with 6 M HCl for hydroxyproline (Hyp) and Gd analysis (15).

Statistical Analysis

All data are shown as means (± SEM). Differences among groups were tested with repeated measures ANOVA, followed by Student-Newman-Keuls *post hoc* test with P less than 0.05 considered as significant. For correlations, the Pearson correlation coefficient was computed and a t-statistic calculated based on the null hypothesis that the correlation coefficient was zero.

The online supplement contains additional details on methods employed here.

RESULTS

Characterization of Animal Model

A single transtracheal BM instillation recapitulates histopathology consistent with pulmonary fibrosis. Animals initially exhibit an approximate 5% weight loss in association with mild lethargy. The severity of fibrosis was determined by a single pulmonary pathologist using hematoxylin and eosin–, trichrome-, and Sirius red–stained slides, and graded using a published quantitative scoring system that grades pulmonary fibrosis on a scale from 0 to 8 (16). Mice treated with BM showed an average fibrosis score of 5 (± 0.6; range 3–7), whereas sham mice all showed a score of 0. By definition, a score of 5 depicts definite damage to lung architecture and formation of fibrous bands or small fibrous masses. Figure 1 shows representative images from sham and BM-treated mice, and demonstrates a pattern of acute subpleural and peribronchial fibrosis. The BM-injured lungs demonstrated a lymphoplasmacytic infiltrate in the areas of fibrosis, along with scattered collagen deposition best visualized with Sirius red. Trichrome staining was less sensitive to detecting collagen deposition. The sham lungs had preserved alveolar architecture, with no collagen deposition or alveolar immune infiltration.

We also quantified the amount of collagen deposition by measuring the relative amount of Sirius red staining in representative slides from each animal. The percentage area of red staining on Sirius red slides was 2.3 times higher for the BM animals compared with the sham animals (sham, 6.8 ± 0.9%; BM, 15.7 ± 1.8%; $P < 0.001$). There was no significant difference in Sirius red staining between the two groups of fibrotic mice that received either EP-3533 or EP-3612.

Quantitative analysis of Hyp was used as a measure of the total amount of collagen in tissue. Hyp levels in BM animals were 35% higher than in sham animals (sham, 73 ± 3 μg Hyp/lung; BM, 99 ± 4 μg Hyp/lung; $P < 0.0001$; Figure 1). There was no significant difference in Hyp concentration between the two groups of fibrotic mice that received either EP-3533 or EP-3612. Together, these results demonstrate that the BM model successfully induces pulmonary fibrosis in mice, accompanied by excessive deposition of collagen, including type I, in the extracellular matrix.

MRI of Pulmonary Fibrosis

We used MRI to characterize the animal model, to assess probe pharmacokinetics, and ultimately to determine whether the collagen-targeted probe, EP-3533, could detect pulmonary fibrosis. We first performed anatomical T1-weighted imaging (RARE) in both coronal and axial orientations. In these images, the lungs are well defined by their negative image contrast (e.g., Figure 2). The lack of signal in the lungs is due to the much lower proton density in the lung compared with other tissue. The air–tissue interface in the lungs results in large magnetic susceptibility gradients that cause signal loss in this type of pulse sequence. However, this RARE sequence is also sensitive to the presence of fluid in the lungs, which results in a positive signal and an opacification of the lungs. Figure 2 compares a sham mouse with a BM mouse, and demonstrates the sensitivity of MRI for edema in this model. Of the BM mice imaged during this study, 8/13 showed presence of pulmonary edema by MRI. Among these animals, presence of edema correlated with higher Hyp content (85 ± 3 μg Hyp/lung versus 104 ± 4 μg Hyp/lung for nonedematous versus edematous; $P = 0.0016$).

To assess the pharmacokinetics of the two probes, we performed a series of MR angiography scans (3D FLASH) before and immediately after intravenous bolus administration of the probe. Figure 3 shows a time course series of coronal images demonstrating the rapid blood clearance of both EP-3533 (*top panel*) and its nontargeted isomer EP-3612 (*bottom panel*). Both probes provide blood pool enhancement immediately after injection, as indicated by the increased signal in the heart and large vessels. By 10 minutes after injection, the blood signal is approaching baseline values. We estimated blood half-life of the probes by drawing an ROI in the jugular vein, measuring the

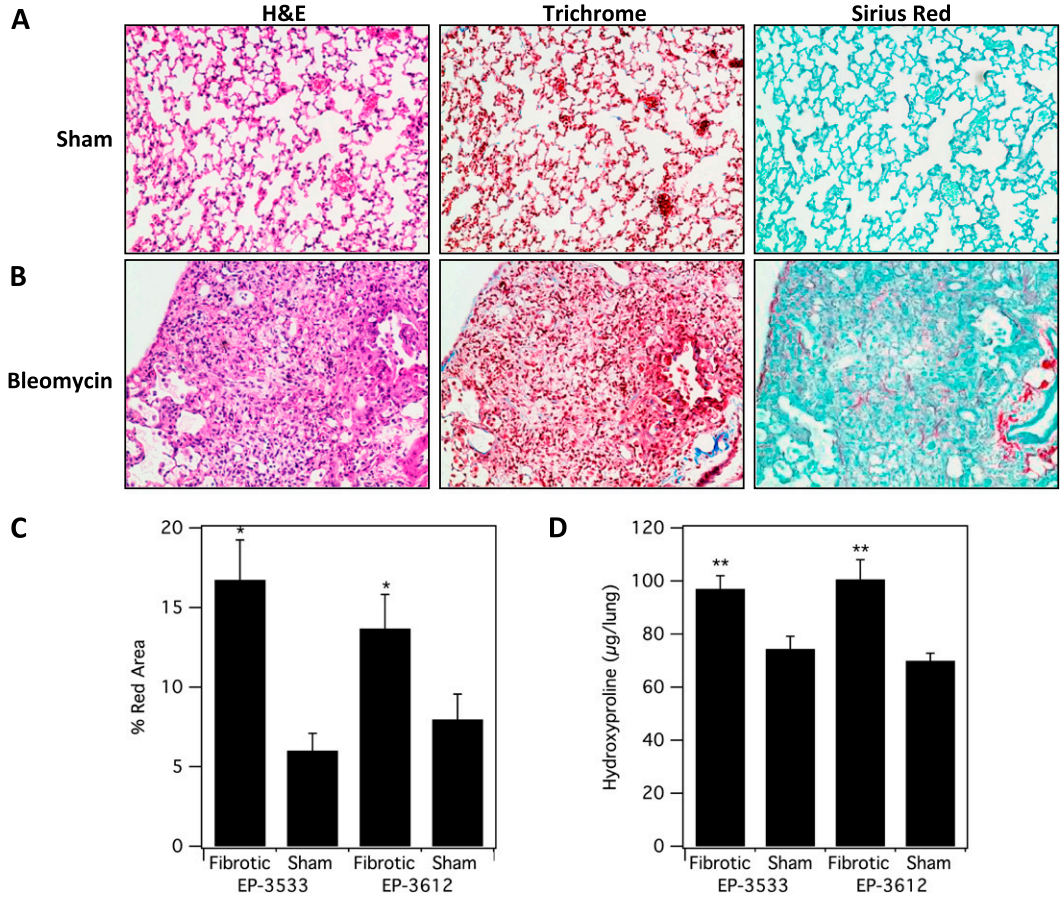

Figure 1. Characterization of fibrosis and collagen deposition in the mouse bleomycin (BM) model. Representative images of lung tissue stained with hematoxylin and eosin (H&E), trichrome, and Sirius red for sham (*A*) and BM-treated mice (*B*). (*C*) Sirius red staining was quantified and was significantly higher in fibrotic (BM-treated) mice (*$P < 0.001$). (*D*) Hydroxyproline (Hyp) analysis of *ex vivo* harvested lung tissue from all four cohorts shows significantly higher Hyp/lung in the fibrotic (BM) -treated cohorts (**$P < 0.0001$).

change in MR SI versus time, and fitting these data to a monoexponential decay. There was no significant difference in blood clearance rate between probes or in probe clearance between BM or sham animals. The mean blood half-life was 8.8 (± 0.7) minutes for EP-3533 and 6.4 (± 0.8) minutes for EP-3612. The kidneys also showed immediate signal enhancement, and this enhancement persisted over 10 minutes, suggesting a predominant renal clearance of both probes.

To circumvent the signal loss in the lung, we used a UTE pulse sequence. This type of sequence is especially effective for tissue with very short T2 relaxation times, such as lung or bone. We used a high flip angle (45°) to provide a more T1-weighted image. This acquisition was performed before probe injection and again starting at 12 minutes after probe injection, after the probe had cleared from the blood pool. Figure 4 shows representative UTE images before probe injection for each of the four cohorts. Superimposed on these images in false color scale is the difference image obtained by subtracting the preprobe UTE image from the post-probe UTE image. All four sets of images are rendered at the same scale. It is apparent from Figure 4 that the signal increase in the lungs of BM mice after targeted EP-3533 probe is much greater than the signal increase in the lungs of sham mice. Figure 4 also shows that the control probe, EP-3612, provides similar and low-signal enhancement in the lungs of either BM or sham mice, and that this signal increase is comparable to EP-3533 in sham mice. These images qualitatively demonstrate the specificity of EP-3533 for pulmonary fibrosis.

To quantify this effect, we measured the change in SNR by drawing ROIs in the lungs and in the shoulder muscle, and comparing the signal in these ROIs in the pre- and post-probe images. ROIs were first drawn in the MR angiography images taken immediately after probe injection to exclude the major vessels in the lungs. These ROIs were then copied to the UTE images and SI changes were computed. The results are summarized in Figure 5. After EP-3533 injection, the lung SNR increased by 34 (± 2)% in the BM mice compared with a 17 (± 2)% increase in sham mice. The untargeted probe, EP-3612, increased lung SNR by 13 (± 1)% in BM mice compared with a 16 (± 1)% increase in sham animals. This twofold higher lung SNR increase in the EP-3533 plus BM mouse cohort was highly significant ($P < 0.0001$). On the other hand, the SNR increase in the muscle was similar among all four cohorts.

The concentration of each probe in the lung and muscle was determined by elemental analysis of Gd *ex vivo* at 60 minutes after injection of probe. The *ex vivo* Gd data mirrored the imaging findings (Figure 5). There was 2.7 times more Gd in fibrotic lungs after EP-3533 compared with the sham mice. Overall, the lung Gd concentrations were highest for the EP-3533 plus BM mouse cohort, and this concentration (2.8 nmol Gd/lung) was significantly higher than the other three cohorts ($P < 0.05$). On the other hand, there was no significant difference in Gd concentration in muscle among the four cohorts. For EP-3533, the concentration was 10.0 (± 1.3) nmol/g in the skeletal muscle of fibrotic mice compared with 9.8 (± 1.9) nmol/g in the sham mice.

We then studied an additional two groups of BM mice with EP-3533 to determine whether the probe could be used to monitor disease progression. The first group was imaged 5–6 days after BM inoculation, whereas the second group was imaged 12–14 days after inoculation. Figure 6 summarizes the imaging and *ex vivo* analyses for these two groups, as well as the mice that were imaged with EP-3533 at 9–11 days after BM inoculation and sham animals imaged with EP-3533. As expected, we see a monotonic increase in lung Hyp with time (Figure 6B).

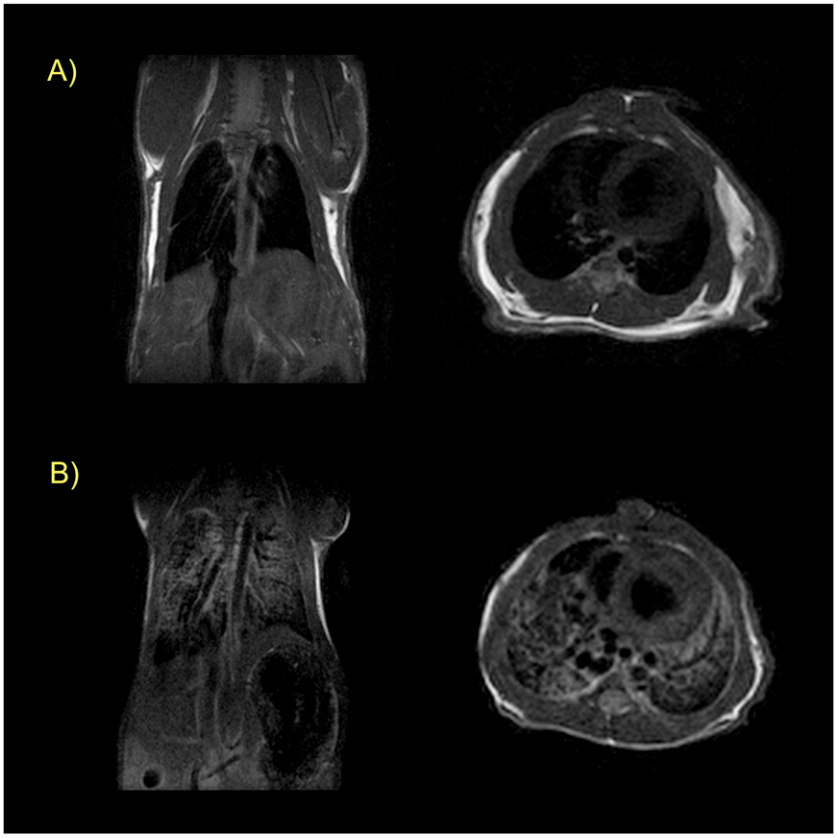

Figure 2. Magnetic resonance (MR) characterization of pulmonary edema. (*A*) Coronal (*left*) and axial (*right*) T1-weighted rapid acquisition with refocused echo (RARE) images of a sham mouse showing absence of signal in the lungs. (*B*) Coronal (*left*) and axial (*right*) images at approximately the same location in a BM-treated mouse. Edema is obvious from the opacification of the lungs in this animal. All images taken before probe injection.

Quantitative scoring of the histology slides also indicated a worsening of disease (2.8 ± 0.2 [range, 2–3] to 5.0 ± 0.6 [range, 3–7] to 5.5 ± 0.3 [range, 5–7] from 5 to 9 to 12 d after BM, respectively). We also observed a monotonic increase in lung signal increase and in *ex vivo* Gd with time after BM (Figures 6A and 6C).

Grouping of animals by time after BM is somewhat arbitrary, because there is a range of disease progression among animals. Therefore, we also looked at the correlation between lung MR signal increase and lung Hyp (as a surrogate for fibrotic severity) for all animals that received EP-3533. There is a strong positive correlation of MR lung signal enhancement and disease progression (Figure 6D). There is also an excellent linear correlation between Hyp and the amount of probe (Gd) measured *ex vivo* in the lung, as well as between signal increase and Gd (Figures 6E and 6F).

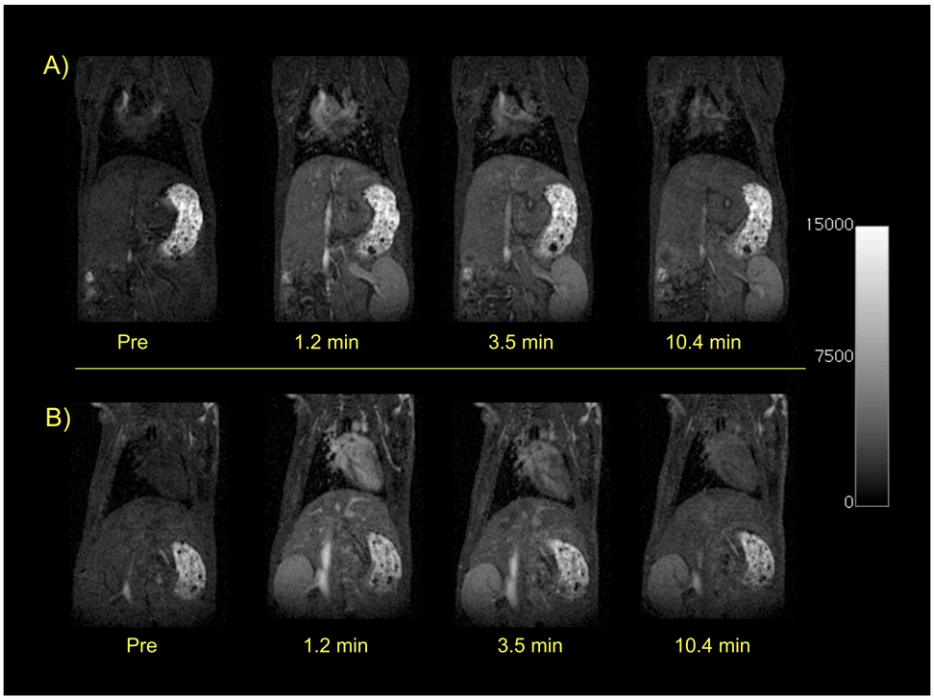

Figure 3. Dynamic T1-weighted MR imaging (MRI) showing rapid renal elimination of the probes. Sham mice before and immediately after intravenous injection of 10 μmol/kg EP-3533 (*top panel*) or EP-3612 (*bottom panel*). Both probes show immediate and similar enhancement of the heart, blood pool, and kidneys. By 10 minutes after injection, the signal in the heart and blood pool is approaching baseline, whereas the kidneys remain enhanced. These dynamic images show the rapid blood clearance and predominant renal elimination pathway that is similar for both EP-3533 and EP-3612.

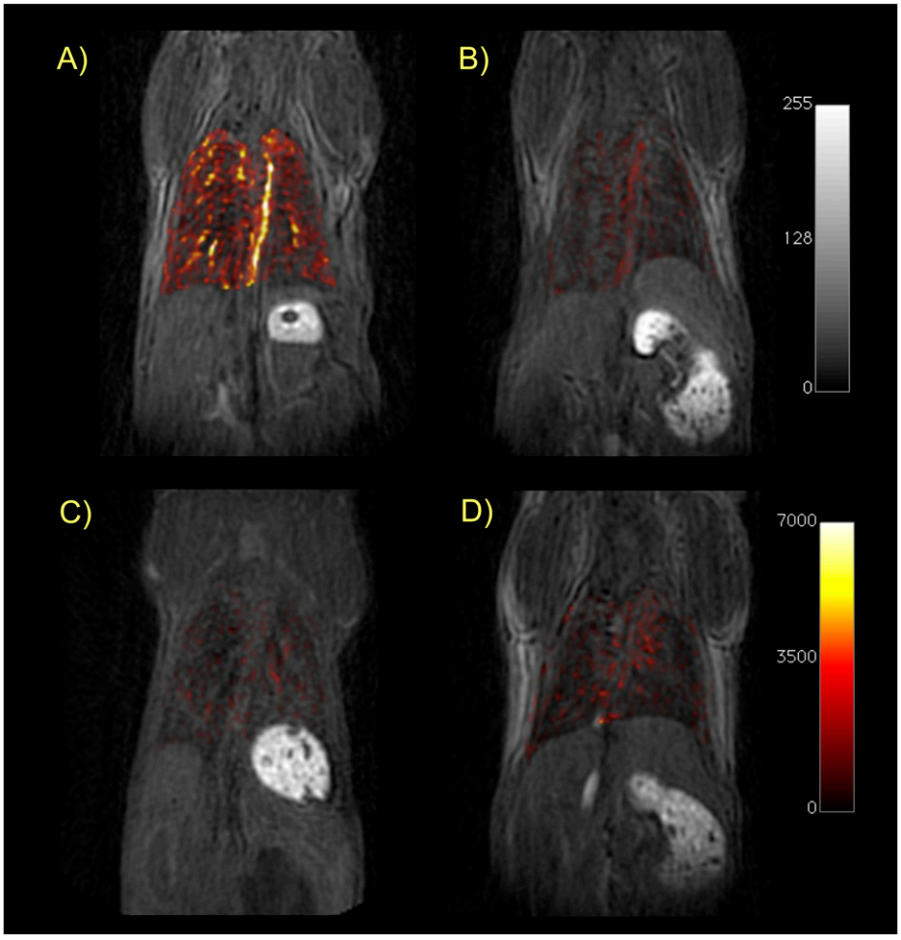

Figure 4. Ultrashort echo time (UTE)-MRI of the lungs. Coronal T1-weighted UTE images of mice from each cohort in this study: (*A*) BM mouse + collagen-targeted EP-3533; (*B*) sham mouse + EP-3533; (*C*) BM + control probe EP-3612; (*D*) sham + EP-3612. *False color overlay* is the difference image obtained by subtracting the UTE image acquired before probe injection from the UTE image taken after probe injection. Mice with pulmonary fibrosis that receive the collagen-specific probe (*A*) show much higher pulmonary signal enhancement than sham mice or mice receiving the control probe. All images rendered at the same scale.

DISCUSSION

IPF is a progressive fibrotic lung disease with a median survival of 2–3 years from the time of diagnosis. The clinical course of IPF, however, is highly variable, with some patients experiencing rapid deterioration and others remaining relatively stable for years (17, 18). There remains a need for better diagnostic tools to predict risk and monitor response to treatment. Therapeutic options for IPF are limited, with the only treatment generally accepted to prolong life being lung transplantation (19). Better diagnostic tools may allow for more appropriate timing of transplantation. In addition, there are a number of new therapies being pursued for IPF (20, 21). Drug development for IPF has been very challenging to date, and there would be value in stratifying patients with respect to their rate of disease progression to enrich trials; it would also be valuable to detect at an early time point whether a therapy is having its intended effect. The heterogeneous nature of lung diseases suggests that systematic measures, including pulmonary function tests (FEV_1) or blood biomarkers, remain nonspecific and may not capture important aspects of the underlying pulmonary disease process, whereas high-resolution molecular imaging may serve that role.

The goal of this study was to determine whether molecular MRI with a collagen-targeted probe was sensitive for pulmonary fibrosis detection in a commonly used BM mouse model. The collagen-targeted probe, EP-3533, was studied in BM and sham mice. To estimate whether the signal enhancement observed with EP-3533 was due to specific collagen binding, we also prepared an isomer, EP-3612. EP-3612 only differs from EP-3533 by the chirality of one cysteine residue, but this mutation abrogates collagen binding in EP-3612. Our study showed that collagen-targeted EP-3533 provided significantly enhanced MR signal in the lungs of fibrotic mice compared with control mice. On the other hand, nonspecific enhancement in the muscle was similar in both fibrotic and control mice. The control probe, EP-3612, showed similar, weak signal enhancement in the lungs of both fibrotic and control mice, demonstrating that the result observed with EP-3533 was due to specific collagen-binding. When we expanded the EP-3533 study to include mice with early stage or more advanced fibrosis, we observed a strong positive correlation of lung MR signal increase with Hyp content, indicating the ability of this probe to stage pulmonary fibrosis.

Proton MRI of the lung is less common owing to the very short T2* relaxation time of the lungs, which results in massive signal loss on standard MR pulse sequences (22). Here, we used a technique called UTE-MR to overcome this limitation and produce positive signal in the lungs. This lung signal could be further increased by the presence of our probe. Although we used a dedicated small animal research scanner, we note that the UTE sequence is widely available on clinical MR scanners, and there is no technological barrier to the translation of this molecular MRI of pulmonary collagen (14, 23).

MR is often not viewed as a molecular imaging technique, primarily because of the relatively high (micromolar) concentrations of probe required to effect signal change. However, type I collagen represents a high-concentration target that is amenable to imaging with an appropriate MR probe. Using MRI, we are able to achieve much higher spatial resolution than positron emission tomography (PET). Here, we acquired images with 250-μm isotropic resolution, which is 64-fold higher than micro-PET scanners ($\sim$ 1 mm isotropic). This high resolution enables easy

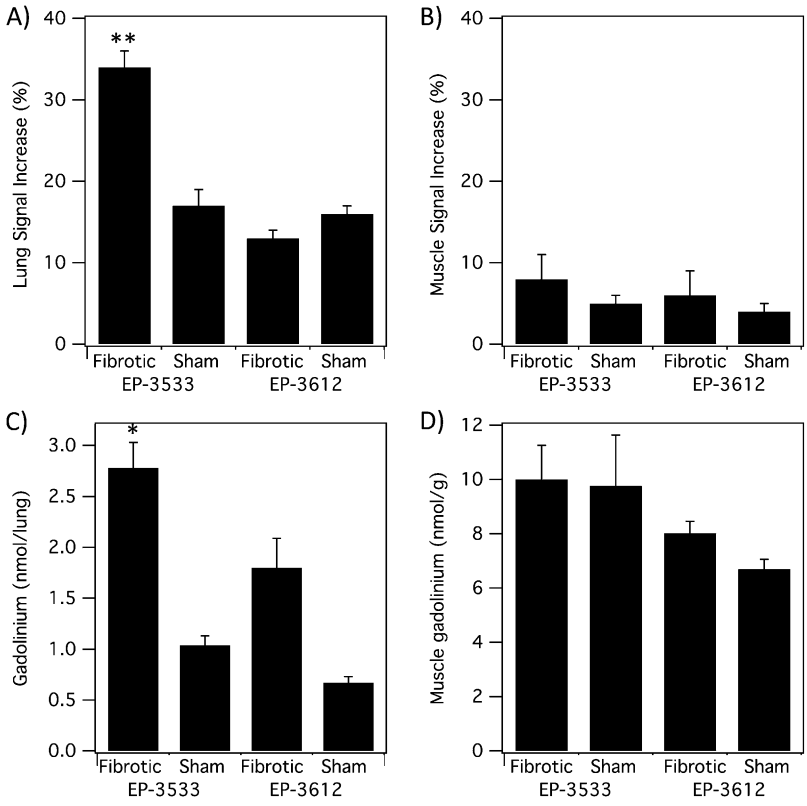

Figure 5. MRI and *ex vivo* analyses. (*A*) Lung signal-to-noise ratio (SNR) increase after probe injection. Fibrotic mice receiving EP-3533 had twofold higher SNR increase compared with sham mice or mice receiving EP-3612 (**$P <$ 0.0001). (*B*) Muscle SNR shows no significant differences between fibrotic and sham animals for either probe. (*C*) *Ex vivo* gadolinium (Gd) analysis shows significantly higher Gd in lungs of fibrotic mice that received EP-3533 compared with sham mice or mice that received EP-3612 (*$P < 0.05$). (*D*) *Ex vivo* Gd concentration in muscle shows no significant differences between fibrotic and sham animals for either probe.

segmentation of the major pulmonary vessels from the lung parenchyma. In this study, high-resolution imaging allowed us to confidently conclude that the signal enhancement observed with the collagen-targeted probe was arising solely from the lung, and was not due to a vascular effect or arising from partial overlap with the liver or heart signal. On clinical scanners, the typical resolution is lower, but MR maintains a much higher spatial resolution than PET. Of further benefit is the lack of ionizing radiation in MR when performing serial imaging to follow disease progression.

The probe, EP-3533, displayed salutary pharmacokinetics for fibrosis imaging. EP-3533 underwent rapid blood clearance with

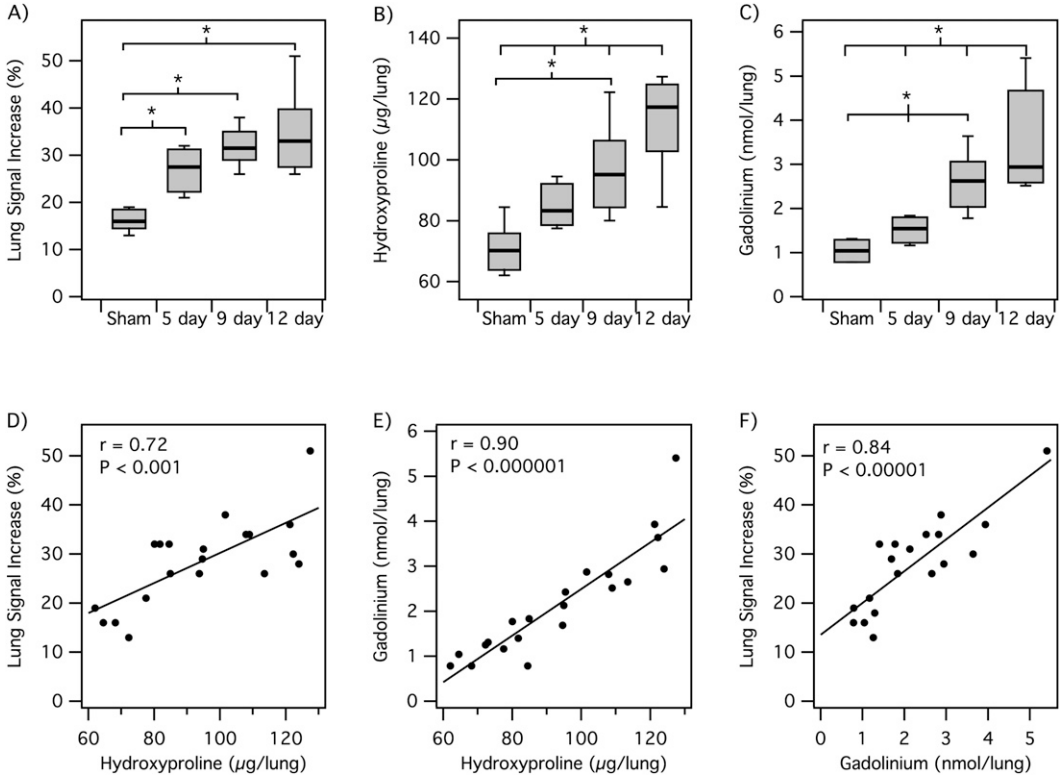

Figure 6. MRI of disease progression. (*A*–*C*) Box plots showing that lung MR signal change after EP-3533 injection (*A*), lung Hyp (*B*), and lung Gd levels (*C*) all increase with time after BM inoculation (*$P < 0.05$). (*D*–*F*) Scatter plots for animals imaged with EP-3533 showing positive linear correlations between lung MR signal increase and lung Hyp (*D*), lung Gd and lung Hyp levels (*E*), and lung MR signal increase and lung Gd (*F*).

renal excretion. The probe is small enough (5 kD) to rapidly penetrate the interstitial space and bind collagen, and the small size and hydrophilic properties of the probe also result in fast renal clearance from the systemic circulation, removing background signal. Such pharmacokinetics allowed fibrosis imaging to take place within 10 minutes of probe injection. The overall Gd dose used was over three times lower than currently used Gd-based contrast media.

HRCT is the radiological gold standard for fibrosis assessment, but not all patients with IPF exhibit clear HRCT patterns of fibrosis. HRCT is less sensitive for the detection of early disease (microscopic fibrinogenesis), where ground glass opacities are often observed and nonspecific. One potential role for a collagen-targeted probe would be to detect fibrosis in this equivocal group. Cystic honeycombing, a late sign of pulmonary fibrosis, is often underestimated by HRCT. A second role would be to monitor changes in fibrosis burden as disease progresses or is treated. High-resolution MRI with a collagen-targeted probe may be sensitive to local disease changes at an early stage before such changes are manifested on HRCT imaging, lung function tests, or in blood biomarkers. Lung biopsy is still part of the diagnostic algorithm in up to 30–60% of patients to distinguish nonspecific interstitial lung disease from usual interstitial pneumonitis, but surgery continues to be associated with a risk of disease exacerbation and mortality (24).

In conclusion, we combined an advanced MRI technique (UTE-MR) with a type I collagen–targeted probe to show that we can distinguish pulmonary fibrosis in a standard mouse model of disease, and monitor its progression. This molecular MRI technique offers the potential of directly imaging collagen and staging pulmonary fibrosis.

Author disclosures are available with the text of this article at www.atsjournals.org.

References

1. Bjoraker JA, Ryu JH, Edwin MK, Myers JL, Tazelaar HD, Schroeder DR, Offord KP. Prognostic significance of histopathologic subsets in idiopathic pulmonary fibrosis. *Am J Respir Crit Care Med* 1998;157:199–203.
2. King TE Jr, Schwarz MI, Brown K, Tooze JA, Colby TV, Waldron JA Jr, Flint A, Thurlbeck W, Cherniack RM. Idiopathic pulmonary fibrosis: relationship between histopathologic features and mortality. *Am J Respir Crit Care Med* 2001;164:1025–1032.
3. Raghu G, Weycker D, Edelsberg J, Bradford WZ, Oster G. Incidence and prevalence of idiopathic pulmonary fibrosis. *Am J Respir Crit Care Med* 2006;174:810–816.
4. Raghu G, Collard HR, Egan JJ, Martinez FJ, Behr J, Brown KK, Colby TV, Cordier JF, Flaherty KR, Lasky JA, *et al*. An official ATS/ERS/JRS/ALAT statement: idiopathic pulmonary fibrosis: evidence-based guidelines for diagnosis and management. *Am J Respir Crit Care Med* 2011;183:788–824.
5. Hunninghake GW, Zimmerman MB, Schwartz DA, King TE Jr, Lynch J, Hegele R, Waldron J, Colby T, Muller N, Lynch D, *et al*. Utility of a lung biopsy for the diagnosis of idiopathic pulmonary fibrosis. *Am J Respir Crit Care Med* 2001;164:193–196.
6. Souza CA, Muller NL, Flint J, Wright JL, Churg A. Idiopathic pulmonary fibrosis: spectrum of high-resolution CT findings. *AJR Am J Roentgenol* 2005;185:1531–1539.
7. Flaherty KR, Travis WD, Colby TV, Toews GB, Kazerooni EA, Gross BH, Jain A, Strawderman RL, Flint A, Lynch JP, *et al*. Histopathologic variability in usual and nonspecific interstitial pneumonias. *Am J Respir Crit Care Med* 2001;164:1722–1727.
8. Monaghan H, Wells AU, Colby TV, du Bois RM, Hansell DM, Nicholson AG. Prognostic implications of histologic patterns in multiple surgical lung biopsies from patients with idiopathic interstitial pneumonias. *Chest* 2004; 125:522–526.
9. Albera C. Challenges in idiopathic pulmonary fibrosis trials: the point on end-points. *Eur Respir Rev* 2011;20:195–200.
10. Caravan P, Das B, Deng Q, Dumas S, Jacques V, Koerner SK, Kolodziej A, Looby RJ, Sun WC, Zhang Z. A lysine walk to high relaxivity collagen-targeted MRI contrast agents. *Chem Commun (Camb)* 2009; 430–432.
11. Caravan P, Das B, Dumas S, Epstein FH, Helm PA, Jacques V, Koerner S, Kolodziej A, Shen L, Sun WC, *et al*. Collagen-targeted MRI contrast agent for molecular imaging of fibrosis. *Angew Chem Int Ed Engl* 2007;46:8171–8173.
12. Helm PA, Caravan P, French BA, Jacques V, Shen L, Xu Y, Beyers RJ, Roy RJ, Kramer CM, Epstein FH. Postinfarction myocardial scarring in mice: molecular MR imaging with use of a collagen-targeting contrast agent. *Radiology* 2008;247:788–796.
13. Polasek M, Fuchs BC, Uppal R, Schuhle DT, Alford JK, Loving GS, Yamada S, Wei L, Lauwers GY, Guimaraes AR, *et al*. Molecular MR imaging of liver fibrosis: a feasibility study using rat and mouse models. *J Hepatol* 2012;57:549–555.
14. Johnson KM, Fain SB, Schiebler ML, Nagle S. Optimized 3D ultrashort echo time pulmonary MRI. *Magn Reson Med* (In press)
15. Hutson PR, Crawford ME, Sorkness RL. Liquid chromatographic determination of hydroxyproline in tissue samples. *J Chromatogr B Analyt Technol Biomed Life Sci* 2003;791:427–430.
16. Ashcroft T, Simpson JM, Timbrell V. Simple method of estimating severity of pulmonary fibrosis on a numerical scale. *J Clin Pathol* 1988;41:467–470.
17. Fernandez Perez ER, Daniels CE, Schroeder DR, St Sauver J, Hartman TE, Bartholmai BJ, Yi ES, Ryu JH. Incidence, prevalence, and clinical course of idiopathic pulmonary fibrosis: a population-based study. *Chest* 2010;137:129–137.
18. Martinez FJ, Safrin S, Weycker D, Starko KM, Bradford WZ, King TE Jr, Flaherty KR, Schwartz DA, Noble PW, Raghu G, *et al*. The clinical course of patients with idiopathic pulmonary fibrosis. *Ann Intern Med* 2005;142:963–967.
19. Thabut G, Christie JD, Ravaud P, Castier Y, Dauriat G, Jebrak G, Fournier M, Leseche G, Porcher R, Mal H. Survival after bilateral versus single-lung transplantation for idiopathic pulmonary fibrosis. *Ann Intern Med* 2009;151:767–774.
20. du Bois RM. Strategies for treating idiopathic pulmonary fibrosis. *Nat Rev Drug Discov* 2010;9:129–140.
21. Wynn TA, Ramalingam TR. Mechanisms of fibrosis: therapeutic translation for fibrotic disease. *Nat Med* 2012;18:1028–1040.
22. Ohno Y, Koyama H, Yoshikawa T, Nishio M, Matsumoto S, Iwasawa T, Sugimura K. Pulmonary magnetic resonance imaging for airway diseases. *J Thorac Imaging* 2011;26:301–316.
23. Ohno Y, Koyama H, Yoshikawa T, Matsumoto K, Takahashi M, Van Cauteren M, Sugimura K. T2* measurements of 3-T MRI with ultrashort TEs: capabilities of pulmonary function assessment and clinical stage classification in smokers. *AJR Am J Roentgenol* 2011; 197:W279–W285.
24. Kaarteenaho R. The current position of surgical lung biopsy in the diagnosis of idiopathic pulmonary fibrosis. *Respir Res* 2013;14:43.